

DOI: 10.1002/cmdc.201100194

Antagonism of the Stat3–Stat3 Protein Dimer with Salicylic Acid Based Small Molecules

Steven Fletcher,^[a] Brent D. G. Page,^[a] Xialoei Zhang,^[b] Peibin Yue,^[b] Zhi Hua Li,^[c] Sumaiya Sharmeen,^[d] Jagdeep Singh,^[a] Wei Zhao,^[b] Aaron D. Schimmer,^[d] Suzanne Trudel,^[c] James Turkson,^{*[b]} and Patrick T. Gunning^{*[a]}

More than 50 new inhibitors of the oncogenic Stat3 protein were identified through a structure–activity relationship (SAR) study based on the previously identified inhibitor S3I-201 ($IC_{50} = 86 \mu\text{M}$, $K_i > 300 \mu\text{M}$). A key structural feature of these inhibitors is a salicylic acid moiety, which, by acting as a phosphotyrosine mimetic, is believed to facilitate binding to the Stat3 SH2 domain. Several of the analogues exhibit higher potency than the lead compound in inhibiting Stat3 DNA binding

activity, with an in vitro IC_{50} range of 18.7–51.9 μM , and disruption of Stat3–pTyr peptide interactions with K_i values in the 15.5–41 μM range. One agent in particular exhibited potent inhibition of Stat3 phosphorylation in both breast and multiple myeloma tumor cells, suppressed the expression of Stat3 target genes, and induced antitumor effects in tumor cells harboring activated Stat3 protein.

Introduction

The signal transducer and activator of transcription 3 (Stat3) protein mediates the relay of extracellular cytokine or growth factor stimulation to the nucleus, where it initiates the expression of gene profiles that promote cell proliferation, differentiation, and cell survival.^[1] In normal cells, Stat3 transcriptional activity is transient and responsive to physiological cues. However, numerous human cancer cell lines, including breast,^[2] prostate,^[3] ovarian,^[4] brain,^[5] and lung^[6] have been found to harbor persistently activated Stat3 protein. Aberrant Stat3 activity is widely acknowledged to be a master regulator of the cancer phenotype and to play a critical role in malignant transformation and tumorigenesis.^[1] Moreover, dysregulated Stat3 transcriptional function has been implicated in the induction of tumor immune tolerance.^[7] Overactivation of Stat3 promotes tumorigenesis by the up-regulation of cell survival proteins, cell cycle regulators and induction of angiogenesis.^[8] Inhibition of Stat3 signaling correlates with suppression of cell transformation, motility, growth, and the induction of apoptosis in malignant cells.^[9] Cell lines that lack aberrant Stat3 activation are more tolerant to Stat3 inhibitors, possibly identifying an irreversible dependence on persistent Stat3 activation for survival in vulnerable cell lines.^[9] Of clinical and therapeutic significance, earlier studies from our research group and others have shown that in vivo administration of inhibitors of Stat3–Stat3 dimerization induce tumor regression in xenograft models.^[10,11] In summary, Stat3 protein is considered an exciting and high-value target for cancer therapeutics.

The canonical view of Stat3 signaling describes latent Stat3 protein (monomeric^[11] or dimeric^[12]) residing predominantly in the cytoplasm. Ligand binding to the extracellular domain of transmembrane receptors induces intracellular activation of tyrosine kinases such as Janus kinases (JAKs). Receptors are phosphorylated on critical tyrosine residues of their cytoplas-

mic domain, creating docking sites for the recruitment of monomeric unphosphorylated Stat3 protein via its SH2 domain. Stat3 is phosphorylated on a key tyrosine residue, Tyr705, which leads to receptor dissociation and the formation of activated Stat3–Stat3 dimers through reciprocal SH2–pTyr705 interactions. After translocation to the nucleus, dimeric Stat3 complexes bind to DNA response elements and promote gene transcription.^[13,14]

Inhibition of constitutive Stat3–Stat3 complexes by disruption of binding interfaces offers significant value as a molecular targeted therapy for cancer treatment.^[10] Disruption of Stat3 complexes has been achieved through SH2 domain binders

[a] Dr. S. Fletcher,⁺ B. D. G. Page,⁺ J. Singh, Prof. P. T. Gunning
Department of Chemistry, University of Toronto Mississauga
Mississauga, ON, L5L 1C6 (Canada)
Fax: (+1) 905-828-5425
E-mail: patrick.gunning@utoronto.ca

[b] X. Zhang, P. Yue, W. Zhao, Prof. J. Turkson
Department of Molecular Biology and Microbiology
Burnett College of Biomedical Sciences
University of Central Florida, Orlando, FL, 32826 (USA)
Fax: (+1) 407-384-2062
E-mail: jturkson@mail.ucf.edu

[c] Z. H. Li, Prof. S. Trudel
Division of Medical Oncology and Hematology
University Health Network
Princess Margaret Hospital, McLaughlin Centre of Molecular Medicine
620 University Ave, Toronto, ON, M5G 2C1 (Canada)

[d] S. Sharmeen, Prof. A. D. Schimmer
Ontario Cancer Institute/Princess Margaret Hospital
610 University Avenue, Toronto, ON, M5G 2M9 (Canada)

[*] These authors contributed equally to this work.

Supporting information for this article is available on the WWW under <http://dx.doi.org/10.1002/cmdc.201100194>: full synthetic protocols, characterization of intermediate compounds, whole-cell tumor data, fluorescence polarization binding data, and EMSA results.

that compete with phosphorylated Stat3 monomers for the phosphotyrosine (pTyr) binding module. Numerous research groups, including our own, have shown that disruption of Stat3 transcriptional activity through dimer disruption leads to suppression of Stat3 gene expression profiles and induction of apoptosis. Stat3 dimers have been effectively disrupted by peptides,^[15] peptidomimetics,^[16] small molecules,^[17] and metal complexes (Figure 1).^[18] Peptidic inhibitors have been derived

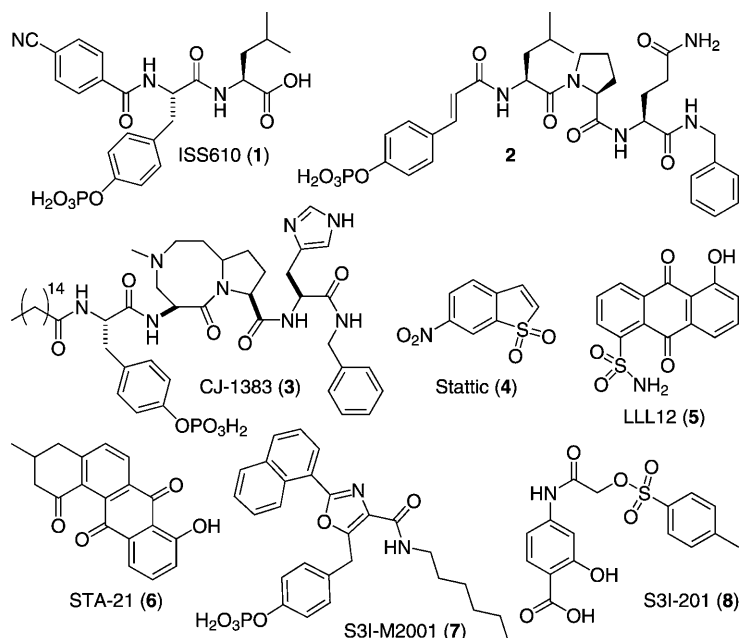


Figure 1. Structures of Stat3 inhibitors 1–8.

from the cognate binding sequence of Stat3 (pYLKTK) and from the Stat3-binding gp130 receptor (GpYLPQTV).^[10] Inspired by these proof-of-principle peptidic probes, our groups^[15a, 16a, d, 17d–g] and many others have synthesized optimized, more drug-like second-generation peptidomimetic inhibitors.^[16b–c, e–g] Most notably, these include ISS610 (4-CN-Ph-pTyr-Leu (1))^[16a] derived from pYLKTK, pCin-Leu-Pro-Glu-NHBn (2)^[16b] derived from GpYLPQTV, and, most recently, the cell-permeable macrocyclic compound CJ-1383 (3).^[16c] In addition to peptidomimetics, small-molecule inhibitors such as Stattec (4),^[17a] LLL12 (5),^[17b] STA-21 (6),^[17c] and S3I-M2001 (7)^[17d, e] have been identified through a combination of *in silico* and *in vitro* screening of chemical libraries as well as *de novo* rational design.

By conducting an *in silico* structure-based virtual screen of the National Cancer Institute (NCI) chemical libraries, our research groups recently identified the potent Stat3 inhibitor S3I-201 (Figure 1, compound 8; $IC_{50} = 86 \mu M$ as determined by an electrophoretic mobility shift assay (EMSA)).^[17f] We identified that S3I-201 offers several opportunities for structural diversification, and embarked on a medicinal chemistry program to identify more potent analogues of S3I-201. Broadly speaking, the Stat3 SH2 domain is composed of three subpockets: a hydrophilic domain bounded by Lys591, Arg609, Ser611, and

Ser613, and two hydrophobic domains; the first comprises Ile634 and the hydrocarbon portions of the side chains of Lys591 and Arg595, and the second comprises Trp623, Val637, Ile659, and Phe716. The structural core of S3I-201 is glycolic acid, the carboxylic acid of which has been condensed with 4-aminosalicylic acid to furnish the amide bond, and the hydroxy group of which has been tosylated. Because S3I-201 carries only two appendages off the main scaffold, GOLD^[19] docking unsurprisingly demonstrated that this small molecule can simultaneously occupy only two of these three subpockets (Figure 2). The salicylic acid moiety of S3I-201 is a known pTyr mimetic,^[20] and low-energy GOLD docking studies consistently placed it in the pTyr binding site. The potential for hydrogen bonds and salt bridges here suggests that this component is responsible for a considerable portion of the binding energy with the Stat3 SH2 domain. GOLD docking studies suggested that the *O*-toluenesulfonyl (tosyl) group binds in the Arg595/Ile634 subpocket, leaving the Trp623/Phe716 subpocket unoccupied; the secondary amide NH of S3I-201 offers an excellent opportunity to gain access to this third subpocket. Thus, we were confident that a rational, synthetic program, facilitated by the inherent modular design of S3I-201, would allow the optimization of contacts between small molecule and the Stat3 SH2 domain to furnish more potent analogues of S3I-201.

The tosylate moiety in S3I-201 is an excellent leaving group, allowing nucleophilic attack at the carbon atom to which it is attached. Moreover, in this case, S3I-201 is especially prone to nucleophilic attack, due to the interaction of the σ^* orbital (the LUMO) of the C–OTs bond with the π^* orbital of the adjacent carbonyl group. Whilst we have no conclusive proof that S3I-201 functions as an irreversible inhibitor, there are several nucleo-

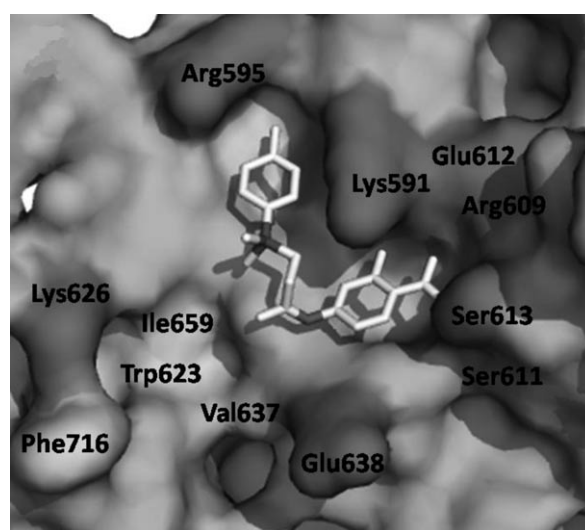


Figure 2. Low-energy GOLD^[19] docking conformation of S3I-201 (8); hydrophobic residues are indicated in light grey, hydrophilic residues are dark grey.

philic residues on the Stat3 SH2 domain surface, including Cys418 and Cys712, that may form a covalent bond to S3I-201. Such an event might compromise an SAR study because the majority of the inhibitory activity would be derived from the irreversible conjugation to the protein surface, which would be common to all S3I-201 analogues. Moreover, it is probable that irreversible inhibitors would exhibit poorer protein selectivity profiles than their reversible inhibitor counterparts. Therefore, we decided to replace the scaffold oxygen atom with a nitrogen atom to convert the labile tosylate into a non-labile tosylamide. The resulting secondary sulfonamide possesses a polar NH group, but despite this, GOLD docking studies consistently placed the tosylamide in the same hydrophobic subpocket (Arg595/Ile634) as the parent tosylate in S3I-201 (compound **9** or SF-1-082,^[16g] Figure 3A). Nevertheless,

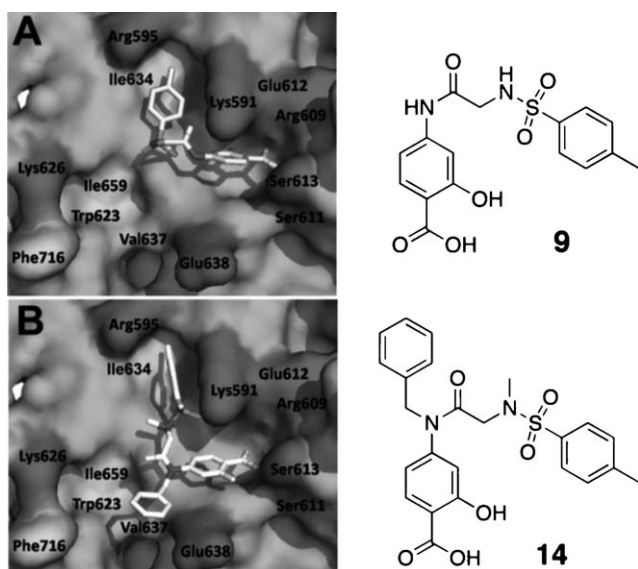


Figure 3. Low-energy GOLD^[19] docking conformations of A) compound **9** and B) compound **14**; hydrophobic residues are indicated in light grey, hydrophilic residues are dark grey.

to further encourage occupancy of this hydrophobic subpocket, we elected to convert the NH group of the tosylamide to the more hydrophobic NCH₃ group. In addition, as alluded to previously, a key aspect of this work was to functionalize the secondary amide NH, as it was anticipated that doing so would allow access to the third, as-yet-unexplored hydrophobic subpocket (Trp623, Val637, Ile659, and Phe716). Indeed, several low-energy GOLD docked poses of the *N*-benzyl derivative **14** (previously reported as SF-1-062)^[16g] revealed that, as well as the salicylic acid and the *N*(CH₃)-tosyl components binding the same subpockets as the corresponding components in the parent S3I-201, the *N*-benzyl group is projected into the third subpocket (Trp623/Phe716) as predicted (Figure 3B).

The *N*(CH₃)-tosylamide analogue of S3I-201 offers four potential optimization sites: 1) the salicylic acid component, 2) the secondary amide NH, 3) the tosyl moiety, and 4) the

N(CH₃) unit of the tosylamide. The salicylic acid moiety is a known phosphotyrosine mimetic, and because its modification would add considerably to the synthetic effort required for this research, we chose to keep this component constant. The remaining three sites would be subjected to SAR studies. Herein we elaborate on our previous communication^[16g] by expanding on the SAR work of our initial lead compound S3I-201 and by providing additional biological characterizations *in vitro* and in whole cells.

Results and Discussion

If the considerable inhibitory activity of S3I-201 is due to its ability to covalently modify the Stat3 target, then conversion of the labile *O*-tosyl group to the non-labile *N*(CH₃)-tosyl group would be expected to cause a significant decrease in the inhibition of Stat3. To investigate this, we first prepared a focused set of non-labile analogues of S3I-201 (shown in Table 1), the

Table 1. EMSA inhibition data for disruption of the Stat3–Stat3:DNA complex *in vitro* by a focused set of S3I-201 (**8**) analogues.

Compd	R ¹	X	IC ₅₀ [μM]
8 (S3I-201)	H	O	86 ± 33
9	H	NH	> 300
10	H	NCH ₃	> 300
11	H	NBoc	> 300
12		O	> 300
13		NH	> 300
14		NCH ₃	292 ± 35
15		NBoc	> 300

syntheses of which are described in full in the Supporting Information. Unfortunately, replacement of the scaffold oxygen atom with NH, NCH₃, or NBoc led to a decrease in activity in all cases, from an IC₅₀ value of 86 μM (by EMSA) to > 300 μM for all non-labile analogues, suggesting that S3I-201 might indeed operate, at least in part, as an irreversible inhibitor. On the other hand, benzylation of the amide NH of S3I-201 also led to a loss in inhibitory activity (compound **12**, SF-1-120:^[16g] IC₅₀ > 300 μM) despite the alkylating potential of this analogue remaining intact. Nevertheless, within this series (R¹ = benzyl), we observed a slight recovery in activity if the scaffold oxygen atom is replaced with the NCH₃ unit (**14**: IC₅₀ = 292 μM), and thus we elected to constrain the X heteroatom/group as NCH₃ for most of this research project. Because **14** demonstrated some activity against Stat3, and we believed the R¹ = benzyl

group of that inhibitor makes favorable interactions with the Trp623/Phe716 hydrophobic subpocket, as predicted by GOLD docking experiments (Figure 3B), we decided to investigate the effects of modifying the benzyl group, in particular at the *para* and *meta* positions, where deeper access to the subpocket might be realized.

Probing the Trp623, Val637, Ile659, and Phe716 hydrophobic subpocket: SAR of the R¹ group

The series of S3I-201 analogues listed in Table 2, where X = NCH₃, were furnished by following the synthetic steps outlined in Scheme 1. After the one-pot and stepwise benzylations of the carboxylic acid and hydroxy functionalities of 4-aminosalicylic acid (**16**), which proceeded in moderate yield (54%), several hydrophobic aldehydes (RCHO) were reductively aminated with the resultant aniline **17** to afford the series of secondary anilines **18** and **19a–i** in very good to excellent yields. Meanwhile, sulfonylation of glycine methyl ester (**20**) with *para*-toluenesulfonyl chloride (*p*-TsCl) furnished secondary sulfonamide **21**, which was subsequently N-methylated with methyl iodide, and then saponified with lithium hydroxide to generate carboxylic acid **23** (75% yield over three steps). Condensation of the primary aniline **17** and the secondary anilines **18** and **19a–i** with acid **23** to deliver the secondary amide **24** and the tertiary amides **25** and **26a–i**, respectively, was achieved with the

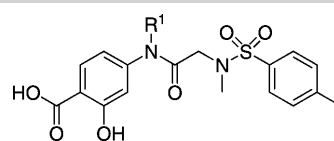
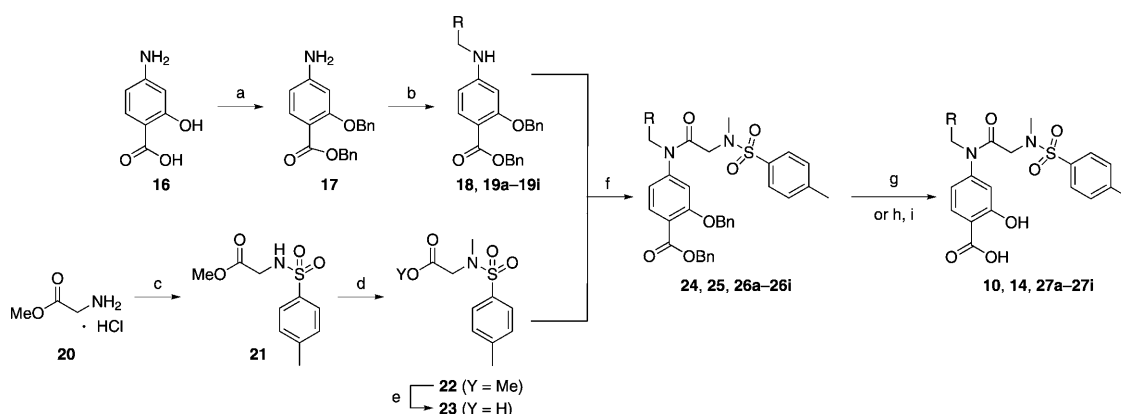


Table 2. EMSA inhibition data for disruption of the Stat3–Stat3:DNA complex in vitro by a series of R¹-functionalized analogues of compound **10**.

Compd	R ¹	IC ₅₀ [μM]	Compd	R ¹	IC ₅₀ [μM]
10	H	> 300	27e		> 300
14		295 ± 35	27f		194 ± 47
27a		290	27g		115 ± 60
27b		> 300	27h		35 ± 9
27c		260 ± 47	27i		280 ± 15
27d		298 ± 11			

highly reactive peptide coupling agent dichlorotriphenylphosphorane (PPh₃Cl₂), which is believed to generate the corresponding acid chloride of **23** in situ. Finally, a global debenzylation of compounds **24**, **25**, and **26a–i** with hydrogen gas over 10% palladium on carbon yielded the series of S3I-201 analogues **10**, **14**, and **27a–i**. Importantly, the aryl nitrile moieties were essentially untouched in the debenzylation reactions, with the reducing conditions proving chemoselective for removal of the benzyl protecting groups. These phenomena are likely due to a combination of rapid reaction times (both aryl



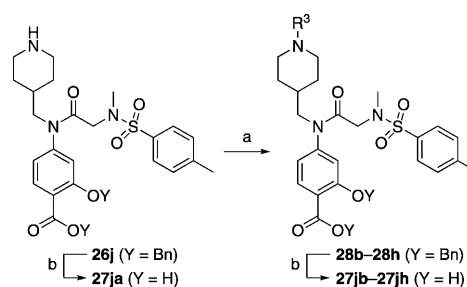
Scheme 1. a) 1. BnBr, KOtBu, DMF, 0 °C → RT, 5 h; 2. BnBr, KOtBu, DMF, 0 °C → RT, 16 h, 54%; b) 1. RCHO, AcOH, 4 Å MS, MeOH, 45 °C, 3 h; 2. NaCNBH₃, RT, 12 h, 75–96%; c) *p*-TsCl, DIPEA, CH₃CN, 0 °C → RT, 1 h, 93%; d) MeI, Cs₂CO₃, DMF, RT, 16 h, 85%; e) LiOH·H₂O, THF/MeOH/H₂O (3:1:1), RT, 1 h, 95%; f) PPh₃Cl₂, CHCl₃, 60 °C, 12 h, 89–95%; g) H₂, 10% Pd/C, MeOH/THF (1:1), RT, 1–16 h, 85–100%; or for **26a** and **26b**: h) LiOH·H₂O, THF/H₂O (3:1), RT, 24 h, 76–86%; i) TFA/toluene (1:2), RT, 16 h, 85–93%.

nitrile-containing intermediates **26c** and **26d** were doubly de-benzylated in ~1 h), which limited the exposure of the nitrile functional group to the reducing conditions, and the fortuitous limited solubilities of the compounds in neat methanol, requiring the use of THF as co-solvent, which is known to suppress hydrogenation of nitriles.^[21] Conversely, because the reduction of aryl–bromide bonds with H₂ and Pd/C catalyst is known to be a relatively facile reaction,^[22] hydrogenolysis of the benzyl protecting groups in intermediates **26a** and **26b** was not attempted. Instead, we employed a high-yielding, non-reducing, two-step protocol. First, the benzyl ester was selectively hydrolyzed with lithium hydroxide (the tertiary amide was slowly hydrolyzed under these conditions), and then the benzyl ether was cleaved under acidic conditions with trifluoroacetic acid (TFA). Removal of the benzyl ether under these conditions is believed to be facilitated by chelation of a proton between the carboxylic acid and ether functionalities.^[23]

Replacement of the R¹ benzyl group in **14** with 4-cyanobenzyl (**27c**, SF-1-073)^[16g] led to an improvement in activity (IC₅₀ = 260 μM for **27c**; cf. IC₅₀ = 292 μM for **14**). This enhancement in Stat3 inhibition may be due to improved hydrophobic interactions with the larger and more electron-poor aromatic system, and/or from a hydrogen bond between the nitrile group and the SH2 domain. More interesting is the observation that Stat3 inhibition improved with increasing size of the hydrophobic R¹ group. Specifically, 4-(*tert*-butyl)benzylated agent **27f** (SF-1-068)^[16g] showed marked improvement in activity over both **14** (R¹ = benzyl) and **27c** (R¹ = 4-cyanobenzyl), whilst replacement of the *tert*-butyl group with a phenyl ring to give the large biphenyl-based inhibitor **27g** (SF-1-070, R¹ = 4-phenylbenzyl) led to a further approximate twofold increase in potency (**27g**, IC₅₀ = 115 μM; cf. IC₅₀ = 194 μM for **27f**). Furthermore, the inclusion of the especially hydrophobic 4-cyclohexylbenzyl group at the R¹ position furnished an inhibitor that exhibited Stat3 inhibitory activity with more than double the potency of our lead agent: IC₅₀ = 35 μM for **27h** (SF-1-066),^[16g] cf. IC₅₀ = 86 μM for S3I-201 (**8**).

N-Substituted piperidinylmethyl derivatives and N-substituted 4-(piperidinyl)benzyl derivatives

Because greater Stat3 inhibitory activity was furnished by substitution at the *para* position of the R¹ benzyl group in **14**, we were keen to functionalize this position further still. However, owing to a simpler synthetic demand, it was decided to determine whether substitution at the 4-position of the cyclohexyl group (a good match for benzyl) would also enhance inhibitor activity. Replacement of the cyclohexylmethyl moiety in **27e** with 4-piperidinylmethyl would allow facile elaboration of the inhibitor through functionalization of the piperidine nitrogen to probe deeper into the proposed subpocket. To this end, compound **26j** (Scheme 2) was accessed by following the steps in Scheme 1, where the RCHO aldehyde was *N*-Boc-piperidinylformaldehyde (the Boc group was inadvertently removed during the peptide coupling step with PPh₃Cl₂; full details for the synthesis of **26j** are given in the Supporting Information). Because the piperidinylmethyl group was proposed to bind in



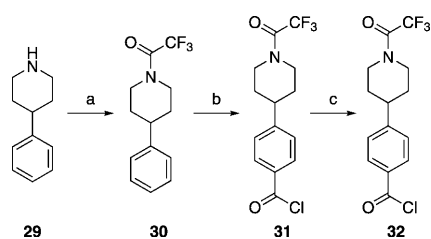
Scheme 2. a) R³ = Boc: Boc₂O, cat. DMAP, CH₂Cl₂, RT, 1 h, 95%; R³ = aryl: R³F or R³Cl, DIPEA, DMSO, 120 °C, 16 h, 76–96%; b) H₂, 10% Pd/C, MeOH/THF (1:1), RT, 1–16 h, 85–100%.

a hydrophobic subpocket, we appreciated that conjugation of groups to the piperidine nitrogen that would considerably decrease its basicity would be required. Thus, the transformations conducted on the piperidine nitrogen (Scheme 2) included *tert*-butoxycarbonylation and arylation with 4-fluorobenzonitrile or 2-chloropyrimidine to afford, after benzyl deprotections, inhibitors **27jb**, **27jc**, and **27jd**, respectively. Unfortunately, as shown in Table 3, none of the inhibitors were active; all exhibited EMSA IC₅₀ values > 300 μM.

Table 3. EMSA inhibition data for disruption of the Stat3–Stat3:DNA complex *in vitro* by a series of R¹ = *N*-(4-piperidinyl)methyl-based analogues of compound **10**.

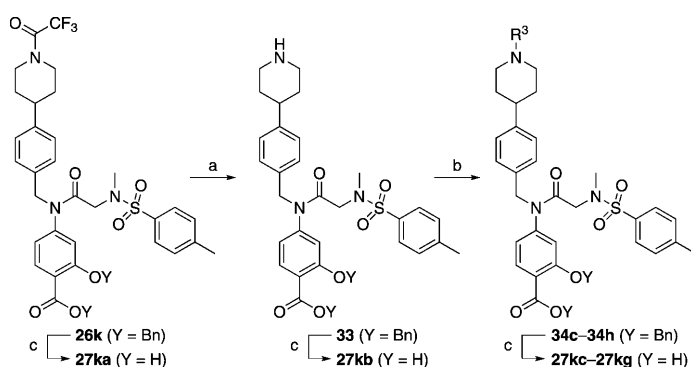
Compd	R ³	IC ₅₀ [μM]
27ja	H	> 300
27jb		> 300
27jc		> 300
27jd		> 300

Next, we tackled functionalization of the 4-position of the cyclohexyl component of inhibitor **27h** in a similar manner. This time, preparation of the requisite aldehyde 4-[*N*-trifluoroacetyl(piperidin-4-yl)]benzaldehyde (**32**) was slightly more complicated, and its synthesis is illustrated in Scheme 3. Briefly, protection of the piperidine nitrogen of 4-phenylpiperidine (**29**) was accomplished as its acid-stable trifluoroacetamide **30**. Subsequently, regioselective *para*-chlorocarbonylation of **30** was effected under Friedel–Crafts conditions,^[24] and then the crude acid chloride **31** was reduced to the target aldehyde **32** in a modification of the Rosenmund reaction. Employing **32** as



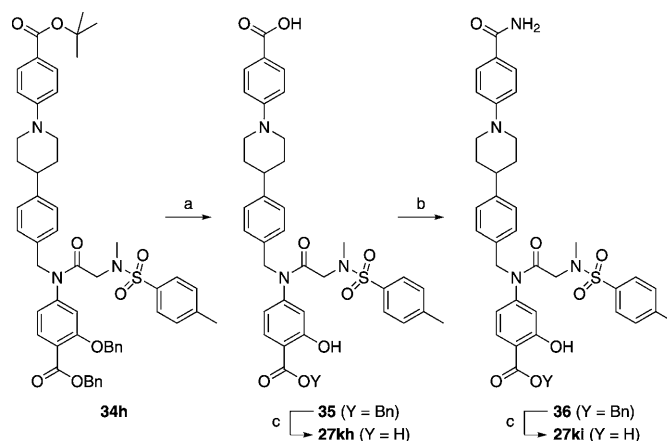
Scheme 3. a) $(\text{CF}_3\text{CO})_2\text{O}$, DIPEA, CH_2Cl_2 , $0^\circ\text{C}\rightarrow\text{RT}$, 3 h, 93%; b) $(\text{COCl})_2$, AlCl_3 , CH_2Cl_2 , 0°C , 1 h; c) H_2 , 10% Pd/C, DIPEA, EtOAc, RT, 2 h, 63% (two steps).

the RCHO aldehyde, the corresponding compound **26k** was then furnished by following the appropriate steps in Scheme 1. Next, as shown in Scheme 4, the trifluoroacetyl group of **26k** was cleaved in excellent yield by brief treatment with lithium hydroxide to reveal the piperidine nitrogen atom



Scheme 4. a) $\text{LiOH}\cdot\text{H}_2\text{O}$, $\text{THF}/\text{H}_2\text{O}$ (3:1), RT, 10 min, 98%; b) $\text{R}^3 = \text{Boc}$: Boc_2O , cat. DMAP, CH_2Cl_2 , RT, 1 h, 95%; $\text{R}^3 = \text{aryl}$: R^3F or R^3Cl , DIPEA, DMSO, 120°C , 16 h, 80–99%; $\text{R}^3 = p\text{-CNC}_6\text{H}_4\text{SO}_2$: $p\text{-CNC}_6\text{H}_4\text{SO}_2\text{Cl}$, DIPEA, RT, 16 h, 99%; $\text{R}^3 = p\text{-CNC}_6\text{H}_4\text{CO}_2$: $p\text{-CNC}_6\text{H}_4\text{CO}_2\text{H}$, HBTU, DIPEA, DMF, RT, 16 h, 89%; c) H_2 , 10% Pd/C, MeOH/THF (1:1), RT, 1–16 h, 85–100%.

in **33**. Subsequent functionalization of this nitrogen was accomplished with a variety of reagents to furnish, after the standard benzyl deprotections, the series of compounds **27ka–kg** depicted in Table 4. As in the case of the *N*-piperidinylmethyl series of inhibitors **27ja–jd**, we elected to substitute the piperidine nitrogen atom in **33** with functionalities that would decrease its basicity through withdrawal of its lone pair of electrons into aryl systems, and acyl and sulfonyl groups. Inhibitors **27kh** and **27ki** were prepared as shown in Scheme 5. Specifically, deprotection of the *tert*-butyl ester of **34h** with TFA also led to the concomitant removal of the benzyl ether, as reported

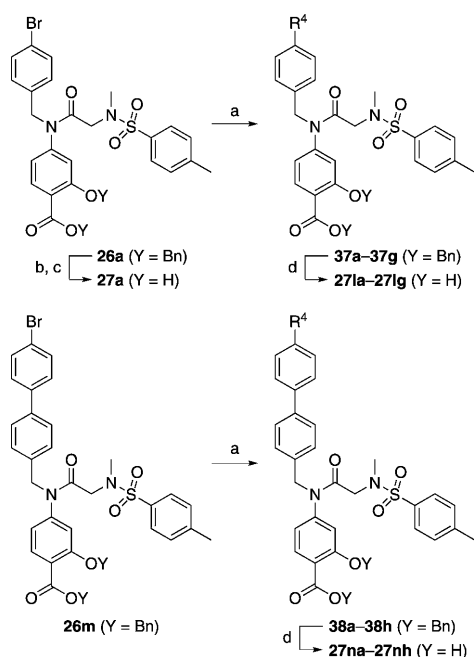


Scheme 5. a) TFA/toluene (1:1), RT, 4 h, 95%; b) NH_4Cl , DIPEA, HBTU, DMF, RT, 16 h, 99%; c) H_2 , 10% Pd/C, MeOH/THF (1:1), RT, 1–16 h, 85–100%.

by us previously, to deliver monobenzyl-protected compound **35**. Facile condensation of the carboxylic acid of **35** with ammonium chloride, employing *O*-(benzotriazol-1-yl)-*N,N,N',N'*-tetramethyluronium hexafluorophosphate (HBTU) as the coupling agent, generated carboxamide **36** in excellent yield. Deprotection of the benzyl esters of **35** and **36** under the usual hydrogenolytic conditions furnished the corresponding inhibitors **27kh** and **27ki**. As the *N*-(piperidin-4-yl)benzyl moiety was predicted to bind in a hydrophobic subpocket, we anticipated that the polar acid and carboxamide-containing inhibitors might demonstrate poor activity against Stat3. In fact, as Table 4 illustrates, among the entire series **27ka–ki**, only 4-cyanophenyl-based **27kd** and 4-cyanobenzene-sulfonyl-based **27kg** exhibited Stat3 inhibitory ac-

Table 4. EMSA inhibition data for disruption of the Stat3–Stat3:DNA complex in vitro by a series of $\text{R}^1 = N$ -(4-piperidinyl)benzyl-based analogues of compound 10.

Compd	R^3	IC_{50} [μM]	Compd	R^3	IC_{50} [μM]
27ka		> 300	27kf		> 300
27kb	H	> 300	27kg		50 ± 15
27kc		> 300	27kah		> 300
27kd		45 ± 12	27ki		> 300
27ke		> 300			



Scheme 6. a) $R^4B(OH)_2$, $Pd(PPh_3)_4$, K_2CO_3 , DMF, $100^\circ C$, 24 h, 16–73%; b) $LiOH \cdot H_2O$, THF/ H_2O (3:1), RT, 24 h, 76–99%; c) TFA/toluene (1:2), RT, 16 h, 85%; d) H_2 , 10% Pd/C, MeOH/THF (1:1), RT, 1–16 h, 85–100%.

tivity ($< 300 \mu M$), with IC_{50} values of 45 and $50 \mu M$, respectively. Both **27kd** and **27kg** share a 4-benzonitrile moiety, so it may seem curious that the related inhibitor 4-cyanobenzamide **27kf** demonstrated no inhibition of Stat3. This result could be due to the nature of the EMSA, which is conducted on nuclear extracts that contain various other members of the STAT protein family. It may be the case that **27kf** is a potent inhibitor of a different STAT isoform, decreasing the concentration of free compound available to inhibit Stat3, leading to an apparent IC_{50} lower than the actual value.

Biphenyl and terphenyl derivatives

After elaborating our inhibitors through functionalization of the 4-position of the cyclohexyl moieties in **27e** ($IC_{50} > 300 \mu M$) and **27h** ($IC_{50} = 35 \mu M$), the next logical approach to probe deeper

into the Trp623/Phe716 hydrophobic subpocket was to modify the biphenyl unit of **27g** ($IC_{50} = 115 \mu M$). The aryl bromide moiety in **26a** provides an excellent handle for facile substitution reactions via Suzuki chemistry, facilitating access to the desired biphenyl analogues of **27g**. To this end, and as described in Scheme 6, **26a** was treated with a variety of aryl boronic acids in the presence of catalytic $Pd(PPh_3)_4$ to furnish, after the standard benzyl group deprotections, the series of *meta*- and *para*-substituted biphenyl-based inhibitors **271a–1h** shown in Table 5. Likewise, the corresponding 4-(4-bromophenyl)benzyl derivative **26m** furnished the terphenyl-based inhibitors **27na–nh** (Table 5).

As shown in Table 5, none of the biphenyl-based inhibitors **271a–271h** offered any improvement in Stat3 inhibitory activity over the parent biphenyl inhibitor **27g** ($IC_{50} = 115 \mu M$). However, excluding the carboxylic acid-substituted compounds **27nb** and **27nf**, the terphenyl-based inhibitors **27na–nh** proved more potent than the parent inhibitor **27g**, with the most active compound **27nh** disrupting the Stat3–Stat3:DNA ternary complex with an IC_{50} value of $43 \mu M$. The improved activity

Table 5. EMSA inhibition data for disruption of the Stat3–Stat3:DNA complex in vitro by a series of biphenyl- and terphenyl-based derivatives of inhibitor **27a**.

Compd	R^4	IC_{50} [μM]	Compd	R^4	IC_{50} [μM]
27g		115 ± 760	27na		63 ± 2
271a		191 ± 8	27nb		> 300
271b		250 ± 23	271c		82 ± 1
271c		> 300	271d		90
271d		> 300	271e		97 ± 17
271e		141 ± 10	271f		> 300
271f		> 300	271g		> 300
271g		> 300	271h		> 300
271h		> 300	27na		63 ± 2
271i		191 ± 8	27nb		> 300
271j		250 ± 23	271c		82 ± 1
271k		> 300	271d		90
271l		> 300	271e		97 ± 17
271m		141 ± 10	271f		> 300
271n		> 300	271g		> 300
271o		> 300	271h		> 300
271p		> 300	27na		63 ± 2
271q		191 ± 8	27nb		> 300
271r		250 ± 23	271c		82 ± 1
271s		> 300	271d		90
271t		> 300	271e		97 ± 17
271u		141 ± 10	271f		> 300
271v		> 300	271g		> 300
271w		> 300	271h		> 300
271x		> 300	27na		63 ± 2
271y		191 ± 8	27nb		> 300
271z		250 ± 23	271c		82 ± 1
272a		> 300	271d		90
272b		> 300	271e		97 ± 17
272c		141 ± 10	271f		> 300
272d		> 300	271g		> 300
272e		> 300	271h		> 300
272f		> 300	27na		63 ± 2
272g		191 ± 8	27nb		> 300
272h		250 ± 23	271c		82 ± 1
272i		> 300	271d		90
272j		> 300	271e		97 ± 17
272k		141 ± 10	271f		> 300
272l		> 300	271g		> 300
272m		> 300	271h		> 300
272n		> 300	27na		63 ± 2
272o		191 ± 8	27nb		> 300
272p		250 ± 23	271c		82 ± 1
272q		> 300	271d		90
272r		> 300	271e		97 ± 17
272s		141 ± 10	271f		> 300
272t		> 300	271g		> 300
272u		> 300	271h		> 300
272v		> 300	27na		63 ± 2
272w		191 ± 8	27nb		> 300
272x		250 ± 23	271c		82 ± 1
272y		> 300	271d		90
272z		> 300	271e		97 ± 17
272aa		141 ± 10	271f		> 300
272ab		> 300	271g		> 300
272ac		> 300	271h		> 300
272ad		> 300	27na		63 ± 2
272ae		191 ± 8	27nb		> 300
272af		250 ± 23	271c		82 ± 1
272ag		> 300	271d		90
272ah		> 300	271e		97 ± 17
272ai		141 ± 10	271f		> 300
272aj		> 300	271g		> 300
272ak		> 300	271h		> 300
272al		> 300	27na		63 ± 2
272am		191 ± 8	27nb		> 300
272an		250 ± 23	271c		82 ± 1
272ao		> 300	271d		90
272ap		> 300	271e		97 ± 17
272aq		141 ± 10	271f		> 300
272ar		> 300	271g		> 300
272as		> 300	271h		> 300
272at		> 300	27na		63 ± 2
272au		191 ± 8	27nb		> 300
272av		250 ± 23	271c		82 ± 1
272aw		> 300	271d		90
272ax		> 300	271e		97 ± 17
272ay		141 ± 10	271f		> 300
272az		> 300	271g		> 300
272ba		> 300	271h		> 300
272bb		> 300	27na		63 ± 2
272bc		191 ± 8	27nb		> 300
272bd		250 ± 23	271c		82 ± 1
272be		> 300	271d		90
272bf		> 300	271e		97 ± 17
272bg		141 ± 10	271f		> 300
272bh		> 300	271g		> 300
272bi		> 300	271h		> 300
272bj		> 300	27na		63 ± 2
272bj		191 ± 8	27nb		> 300
272bj		250 ± 23	271c		82 ± 1
272bj		> 300	271d		90
272bj		> 300	271e		97 ± 17
272bj		141 ± 10	271f		> 300
272bj		> 300	271g		> 300
272bj		> 300	271h		> 300
272bj		> 300	27na		63 ± 2
272bj		191 ± 8	27nb		> 300
272bj		250 ± 23	271c		82 ± 1
272bj		> 300	271d		90
272bj		> 300	271e		97 ± 17
272bj		141 ± 10	271f		

of the terphenyl-based inhibitors over their biphenyl-based counterparts is likely due, at least in part, to enhanced van der Waals contacts between the larger terphenyl moieties and the protein surface, possibly in the proposed Trp623/Phe716 sub-pocket. The observation that the 4-carboxamide terphenyl **27nh** was the most potent of the series is probably due to a hydrogen bond between the carboxamide functional group and the protein surface.

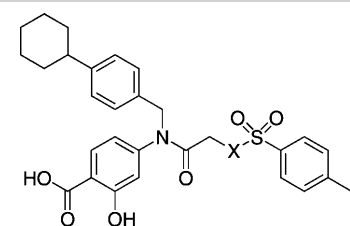
Probing the Arg595/Ile634 hydrophobic subpocket: SAR of the sulfonamide X group

To complete our research program, we modified the X=NCH₃ component (X=O in S3I-201) whilst invoking optimized R¹ and R² groups to help identify even more potent Stat3 inhibitors. Once more, R¹ was constrained as the 4-cyclohexylbenzyl group. Thus, a focused variation of the NCH₃ group in **27h** was executed. The substitutes chosen were the more hydrophobic NBoc group, the more polar NH group, and oxygen, affording, in the latter case, a potentially irreversible inhibitor. The syntheses of these target molecules are depicted in Scheme 7. Briefly, secondary aniline **19h** was coupled to TsN(Boc)CH₂CO₂H (**39**) using PPh₃Cl₂, which, due to the generation of HCl in situ, led to the inadvertent loss of the Boc group to furnish **40**. Standard hydrogenolytic debenzylation of **40** gave **41** (SF-1-083),^[169] or, alternatively, the NH of **40** was re-*tert*-butoxycarbonylated and then debenzylated as usual to deliver **43** (SF-1-087).^[169] To synthesize the labile *O*-tosyl analogue of **41**, compound **19h** was first coupled to 2-acetoxyacetyl chloride to produce **44**. Simple hydrolysis of the acetate group in the presence of the aryl benzyl ester proceeded smoothly. Tosyla-

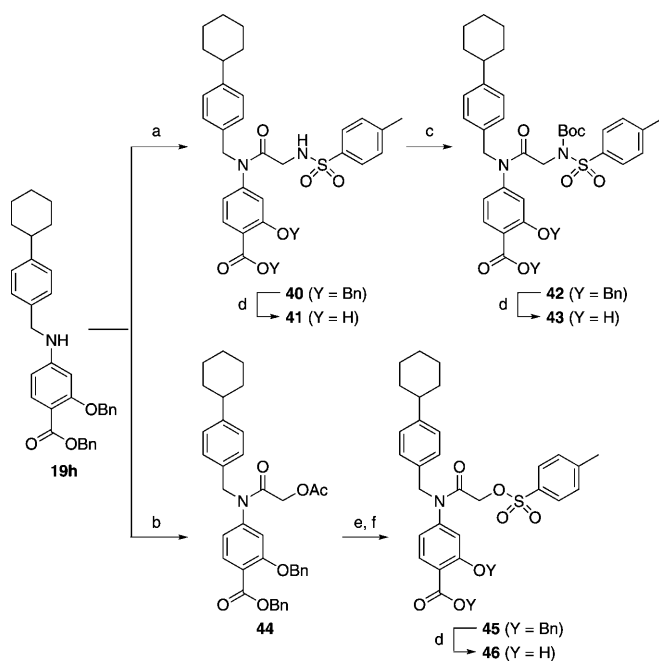
tion of the resultant primary alcohol to give **45** was nontrivial and required the use of 20 equiv *p*-TsCl in order to suppress symmetrical ether formation through the reaction of the starting alcohol with the product tosylate. Debzoylation of **45** was closely monitored, and fresh Pd catalyst (10 mol%) was added every 2 h to minimize reaction time and the likelihood of loss of the *O*-tosyl group through nucleophilic attack by the methanol co-solvent. S3I-201 analogue **46** (SF-1-121)^[169] was thus furnished in very good yield (85%).

The EMSA data for compounds **41** and **43** in Table 6 indicate that changing the X=NCH₃ group in compound **27h** to NH or NBoc, respectively, had a detrimental effect on Stat3 inhibitory activity, increasing the IC₅₀ value from 35 to ~100 μM. However,

Table 6. EMSA inhibition data for disruption of the Stat3–Stat3:DNA complex in vitro by a series of X-substituted *para*-toluenesulfonyl analogues of inhibitor **27h**.



Compd	X	IC ₅₀ [μM]
27h	NCH ₃	35 ± 9
41	NH	95 ± 9
43	NBoc	115 ± 35
46	O	43 ± 13



Scheme 7. a) TsN(Boc)CH₂CO₂H (**46**), PPh₃Cl₂, CHCl₃, 60 °C, 12 h, 48%; b) AcOCH₂COCl, DIPEA, CH₂Cl₂, RT, 4 h, 64%; c) (Boc)₂O, cat. DMAP, THF, 12 h, 81%; d) H₂, 10% Pd/C, MeOH/THF (1:1), RT, 1–16 h, 85–94%; e) LiOH·H₂O, THF/MeOH/H₂O (3:1:1); 89% f) *p*-TsCl, DIPEA, CH₂Cl₂, RT, 3 h, 85%.

er, more interestingly, the *O*-tosyl analogue **46** was equipotent with the parent inhibitor **27h**, within experimental error. Compound **46**, carrying the labile *O*-tosyl group, has the capacity to function as an irreversible inhibitor, whilst **27h**, with the non-labile *N*(CH₃)-tosyl moiety, possesses no such potential. These data thus suggest that the inhibitory activity of **46** likely arises chiefly from noncovalent interactions with the Stat3 SH2 domain. Interestingly, however, the similar activities of **46** and **27h** are in stark contrast to the very different activities of the analogous R¹=H derivatives S3I-201 (**8**) and **10**, respectively, for which replacement of the X=O atom with NCH₃ abolished Stat3 inhibitory activity (> 300 μM). Taken together, these results suggest that the R¹=4-(cyclohexyl)benzyl moiety in **27h** and **46** contributes significantly to the inhibition of Stat3. Furthermore, it is evident that the nature of the X group in the S3I-201 scaffold plays a considerable role in the subsequent Stat3 inhibitory activity, and for this reason our current research efforts are focused toward a more extensive SAR study of this group. This work shall be reported in due course.

We selected several of our analogues of S3I-201 (**8**) for more thorough biophysical characterization by evaluating their inhibition of the Stat3 protein in isolation by using an in vitro fluorescence polarization (FP) assay.^[25] The principle of this assay works on the decrease in FP that occurs upon displacement of the 5-carboxyfluorescein (F*)-labeled Stat3 SH2

Table 7. EMSA and FP inhibition data of selected inhibitors for disruption of the Stat3–Stat3:DNA and Stat3–gp130 sequence complexes in vitro.

Compd	R ¹	X	R ²	EMSA IC ₅₀ [μM]	FP K _i [μM]
8 (S3I-201)	H	O		86 ± 33	> 50
27 h		NCH ₃		35 ± 9	15 ± 4.9
27 kd		NCH ₃		45 ± 12	18.7 ± 1.4
27 kd		NCH ₃		50 ± 15	21.5 ± 2.2
27 kd		NCH ₃		74.3 ± 9.3	21.6 ± 0.9
27 kd		NCH ₃		43 ± 1.3	16.7 ± 1.7

domain inhibitor F*-GpYLPQTV from the Stat3 protein by the small molecule of interest. Generally, the FP K_i data for the selected inhibitors (Table 7) corroborate those data observed in the EMSA, with potent activity in one assay reflected by potent activity in the other. These data support our hypothesis that the S3I-201 analogues disrupt the ternary Stat3–Stat3:DNA complex, as quantified in the EMSA, through direct inhibition of the Stat3 protein. It is reasonable to expect that disruption of the Stat3–Stat3 dimer (full-length protein) bound to DNA in the EMSA may be more difficult than disrupting the Stat3–phosphopeptide interaction in the FP assay, and this is probably the reason why, in many cases, the FP-determined K_i values were lower than the corresponding EMSA-determined IC₅₀ values.

STAT isoform selectivities

Using a similar Stat1 SH2 domain FP-based binding assay,^[26] we also investigated the isoform selectivity of some of our most potent Stat3 inhibitors by evaluating their inhibitory ac-

tivities against Stat1, which exhibits 78% sequence identity to Stat3.^[27] The results of our findings are disclosed in Table 8 and in the Supporting Information. Compound **27 h** exhibited a greater than threefold selectivity for Stat3 (Stat3: K_i = 15 μM, Stat1: K_i ≥ 50 μM). In contrast to **27 h**, the 4-cyanobenzenesulfonyl-based compound **27 kg** showed only limited isoform specificity (Stat3: K_i = 21 μM, Stat1: K_i = 28 μM), which, given the structural similarities of these two compounds, suggests that the 4-cyclohexylbenzyl group at the R¹ position is also a source of Stat3 isoform specificity.

Whole-cell cytotoxicity

Agents **27 h**, **27 kd**, **27 kg**, **27 nh**, and **46** all show significantly improved in vitro inhibitory activity against Stat3 DNA binding activity (as determined by EMSA), with IC₅₀ values of 18.7–51.9 μM (Tables 5–8) and Stat3–pTyr peptide interaction in the FP assay, with K_i values of 13–26.5 μM (Tables 7 and 8 and Supporting Information). For select active compounds, whole-cell activities were investigated by screening inhibitors at a concentration of

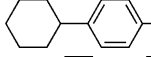
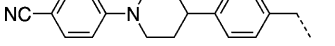
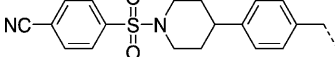
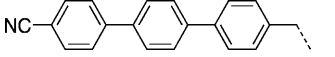
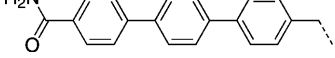
up to 100 μM across a range of human tumor cell lines, namely breast cancer (MDA-MB-468),^[28] prostate cancer (DU145),^[29] acute myeloid leukemia (OCI-AML-2),^[30] and human multiple myeloma (JLN-3), all of which harbor constitutively active Stat3 (data not shown). The inhibitory activities (IC₅₀ values) for select compounds are listed in Table 9.

Indeed, there was good correlation between the whole-cell effects and the inhibition of Stat3 in nuclear extracts. Treatment of cells with compounds **10**, **14**, **27 a–e**, **27 i**, **27 ja–jd**, **27 ld**, **27 lh**, and **27 nd** had no effect on cell growth at inhibitor

Table 8. Comparative Stat isoform selectivity as assessed by a Stat3 and Stat1 FP assay.

Compd	K _i [μM]	
	Stat3	Stat1
27 h	15 ± 5	> 50
27 kd	8.4 ± 1	> 50
27 kg	21 ± 2	28 ± 2
27 nh	8.4 ± 2	9.5 ± 2

Table 9. IC₅₀ values for selected R¹-substituted analogues in whole-cell viability studies.


Compd	R ¹	MDA-MB-468 ^[a]	IC ₅₀ [μM] DU145 ^[b]	OCI-AML-2 ^[c]
27h		17 ± 4	37 ± 12	36 ± 13
27kd		> 100	> 100	> 100
27kg		95 ± 9	> 100	> 100
27ng		33 ± 16	94 ± 7	58 ± 14
27nh		> 100	> 100	> 100

[a] MDA-MB-468: breast cancer. [b] DU145: prostate cancer. [c] OCI-AML-2: acute myeloid leukemia.

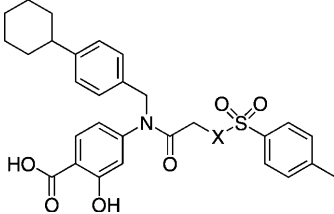
concentrations < 100 μM, reflecting their poor IC₅₀ values in the EMSA (data not shown), whereas the active Stat3 inhibitors in the *in vitro* EMSA inhibited the growth of cells dependent on constitutively active Stat3. Accordingly, the whole-cell activities observed with **27h**, **27kg**, and **46** mirror their inhibitory activities in the Stat3 DNA binding activity/EMSA (Table 2) and the Stat3-pTyr peptide interactions in the FP assay (Tables 7 and 8). Agent **27h** inhibited the growth of MDA-MB-468 breast cancer cells with an IC₅₀ value of 17 μM, of DU145 with IC₅₀ = 37.2 μM, and of OCI-AML-2 with IC₅₀ = 35.9 μM, consistent with its EMSA results or the K_i value for the inhibition of Stat3-pTyr peptide interactions (Tables 7 and 8). Notably, although **27h** inhibited Stat3 activity in EMSA with an IC₅₀ value of 35 μM, it inhibited Stat3-pTyr peptide interactions with an IC₅₀ value of 15 μM (Table 8), suggesting that in cells, it might be more effective to disrupt Stat3 binding to pTyr peptide motifs of receptors, as has been previously reported for dimerization disruptors by our group.^[15,17g] Consistent with the findings from the EMSA (Tables 3 and 4), the *N*-(4-piperidinyl)methyl- (**27ja–27d**) and *N*-(4-piperidinyl)benzyl-based (**27ka–kf**) inhibitors proved ineffective toward the growth of Stat3-dependent tumor cell lines.

Generally, a good correlation was observed between the EMSA data for the biphenyl- and terphenyl-based compounds (Table 5) and the whole-cell data for the Stat3-dependent cell lines, particularly with the MDA-MB-468 cell line. It is probable that the polar carboxamide functional groups in **27nd** and **27nh** hindered cellular entry of these compounds, hence their poorer whole-cell activities than might have otherwise been anticipated based on their activities in the EMSA. Generally speaking, these series of compounds were equipotent at inhibiting the growth of breast cancer MDA-MB-468 cells and acute myeloid leukemia OCI-AML-2 cells, and were around half as

active or worse in the prostate cancer DU145 cell line. Compound **27h** shows strong cellular effects (Table 10), consistent with the inhibition of Stat3 activity in cells (Figure 4).

As detailed in Table 10, analogues of S3I-201 (**8**) carrying the optimized R¹ = 4-cyclohexylbenzyl and R² = *p*-tolyl groups all exhibited sub-100 μM activities in the three Stat3-dependent tumor cell lines. Compounds **27h** (X = NCH₃) and **41** (X = H) were roughly equipotent. The most potent compound of this series in the Stat3-dependent cell lines was compound **43**, the X = NBoc analogue of **27h**, inhibiting MDA-MB-468 cell growth with an IC₅₀ value of 10.5 μM. The improved whole-cell activities of **43** relative to **27h** is possibly due to the greater hydrophobicity of the NBoc group over the NCH₃ group, which might facilitate more efficient cellular entry. Encouragingly, when assessed by FP for Stat3 binding potency, compound **43** was shown to have K_i = 15 ± 0.2 μM (Supporting Information). The *O*-tosyl derivative **46**, a potentially irreversible inhibitor, demonstrated activities in the Stat3-dependent cell lines that were around half that exhibited by the parent **27h**. These findings may, in part, be a consequence of the possible hydrolysis of **46** to primary alcohol **47**, which was synthesized and found to show no inhibition of Stat3 *in vitro* (IC₅₀ > 300 μM), nor appreciable whole-cell activity (MDA-MB-468: IC₅₀ > 100 μM).

concentrations < 100 μM, reflecting their poor IC₅₀ values in the EMSA (data not shown), whereas the active Stat3 inhibitors in the *in vitro* EMSA inhibited the growth of cells dependent on constitutively active Stat3. Accordingly, the whole-cell activities observed with **27h**, **27kg**, and **46** mirror their inhibitory activities in the Stat3 DNA binding activity/EMSA (Table 2) and the Stat3-pTyr peptide interactions in the FP assay (Tables 7 and 8). Agent **27h** inhibited the growth of MDA-MB-468 breast cancer cells with an IC₅₀ value of 17 μM, of DU145 with IC₅₀ = 37.2 μM, and of OCI-AML-2 with IC₅₀ = 35.9 μM, consistent with its EMSA results or the K_i value for the inhibition of Stat3-pTyr peptide interactions (Tables 7 and 8). Notably, although **27h** inhibited Stat3 activity in EMSA with an IC₅₀ value of 35 μM, it inhibited Stat3-pTyr peptide interactions with an IC₅₀ value of 15 μM (Table 8), suggesting that in cells, it might be more effective to disrupt Stat3 binding to pTyr peptide motifs of receptors, as has been previously reported for dimerization disruptors by our group.^[15,17g] Consistent with the findings from the EMSA (Tables 3 and 4), the *N*-(4-piperidinyl)methyl- (**27ja–27d**) and *N*-(4-piperidinyl)benzyl-based (**27ka–kf**) inhibitors proved ineffective toward the growth of Stat3-dependent tumor cell lines.

Table 10. IC₅₀ values for a series of *para*-toluenesulfonyl X analogues of inhibitor **27h** in whole-cell viability studies.


Compd	X	IC ₅₀ [μM]		
		MDA-MB-468 ^[a]	OCI-AML-2 ^[b]	DU145 ^[c]
27h	NCH ₃	17 ± 4	37 ± 12	36 ± 13
41	NH	21 ± 6	38 ± 14	33 ± 8
43	NBoc	10 ± 9	24 ± 16	18 ± 9
46	O	43 ± 6	52 ± 13	62 ± 12

[a] MDA-MB-468: breast cancer. [b] OCI-AML-2: acute myeloid leukemia. [c] DU145: prostate cancer.

Inhibition of intracellular aberrant Stat3 phosphorylation and the induction of known Stat3-regulated genes

Consistent with the effects on viability, **27h** strongly inhibited constitutively active Stat3 in tumor cells, including the human breast cancer (MDA-MB-468) and multiple myeloma (JJN-3) lines, as measured by Western blot analysis (Figure 4A), con-

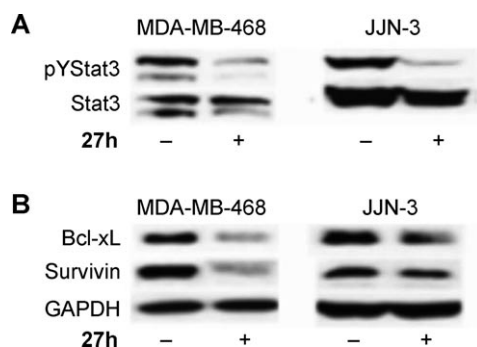


Figure 4. Western blot analysis showing A) inhibition of Stat3 phosphorylation (pYStat3) and B) repression of Stat3-regulated gene products, Bcl-xL and Survivin, in human breast (MDA-MB-468) and multiple myeloma (JJN-3) cells as a function of treatment with **27h** (100 μ M, 24 h). Glyceraldehyde 3-phosphate dehydrogenase (GAPDH) was used as a lane loading control.

firming that select agents inhibit aberrant Stat3 activation in tumor cells. Furthermore, treatment with **27h** inhibited the expression of Bcl-xL and Survivin, the genes for which are known to be regulated by Stat3 (Figure 4B). These findings suggest that the modulation of aberrant Stat3 in MDA-MB-468 and JJN-3 cells leads to suppression of Stat3-mediated gene regulation. These events contribute to the loss of viability observed following the treatment of malignant cells that harbor aberrant Stat3 activity by the newly identified small-molecule inhibitors.

Conclusions

In summary, we have conducted an extensive SAR study centered on the previously identified Stat3 inhibitor S31-201 (**8**) to derive analogues with improved Stat3 inhibitory activity. These studies have led to the identification of several diverse classes of agents equipped with an additional appendage that promotes interaction with the hitherto unexplored pocket on the Stat3 protein surface, thereby intensifying the binding to Stat3 and enhancing the Stat3 inhibitory activity. Specifically, compounds **27h**, **27nh**, **27kd**, **27kg**, and **46** all show significantly improved in vitro inhibitory activity against Stat3, with IC_{50} values of 18.7–51.9 μ M. Moreover, at these concentrations, select compounds inhibit constitutively active Stat3 and Stat3 tyrosine phosphorylation in malignant cells and promote anti-tumor cell effects consistent with the inhibition of aberrant Stat3 activity. The improved inhibitory activity against Stat3 activation is derived in part from the successful occupation of the third subdomain of the Stat3 SH2 domain, as supported by computational modeling; S31-201 can simultaneously occupy

only two of these subdomains. Importantly, with a labile *O*-tosyl group α to a carbonyl group, S31-201 has the capacity to operate, at least in part, as an irreversible inhibitor, which would be anticipated to lead to poor protein selectivity profiles.

Experimental Section

Anhydrous solvents MeOH, DMSO, CH_2Cl_2 , THF, and DMF were purchased from Sigma–Aldrich and were used directly from Sure-Seal bottles. Molecular sieves were activated by heating at 300 °C under vacuum overnight. All reactions were performed under an atmosphere of dry N_2 in oven-dried glassware and were monitored for completeness by thin-layer chromatography (TLC) using silica gel (visualized by UV light, or developed by treatment with $KMnO_4$ stain or phosphomolybdic acid stain). 1H and ^{13}C NMR spectra were recorded on Bruker 400 MHz and Varian 500 MHz spectrometers in either $CDCl_3$, CD_3OD , or $[D_6]DMSO$. Chemical shifts (δ) are reported in ppm after calibration to residual isotopic solvent. Coupling constants (*J*) are reported in Hz. Before biological testing, inhibitor purity was evaluated by reversed-phase HPLC (RP-HPLC). Analysis by RP-HPLC was performed by using a Microsorb-MV 300A C_{18} 250 \times 4.6 mm column run at 1 mL min^{-1} , and using gradient mixtures of A) H_2O with 0.1 M CH_3COONH_4 and B) MeOH. Ligand purity was confirmed by using linear gradients from 75% A and 25% B to 100% B after an initial 2 min period of 100% A. The linear gradient consisted of a changing solvent composition of either I) 4.7% per minute and UV detection at λ 254 nm, or II) 1.4% per minute and detection at λ 214 nm, each ending with 100% B for 5 min. For reporting HPLC data, percentage purity is given in parentheses after the retention time for each condition. All biologically evaluated compounds are of >95% chemical purity as measured by HPLC. Full characterization for all final compounds and intermediate compounds are provided in the Supporting Information.

Acknowledgements

We thank Jeffrey L. Wrana and Alessandro Datti (Mt. Sinai Hospital) for access to the SMART high-throughput screening facility. This work was supported by the Leukemia and Lymphoma Society of Canada (P.T.G.), NSERC (P.T.G.), the University of Toronto (P.T.G.), and by National Cancer Institute grants CA106439 (J.T.) and CA128865 (J.T.). A.S. is a Leukemia and Lymphoma Society Scholar in Clinical Research.

Keywords: antitumor agents • molecular recognition • molecular therapeutics • protein–protein interactions • stat3

- [1] a) R. Buettner, L. B. Mora, R. Jove, *Clin. Cancer Res.* **2002**, *8*, 945–954; b) J. E. Darnell, Jr., *Nat. Med.* **2005**, *11*, 595–596; c) T. Bowman, R. Garcia, J. Turkson, R. Jove, *Oncogene* **2000**, *19*, 2474–2488.
- [2] M. Berishaj, S. P. Gao, K. Leslie, H. Al-Ahmadie, W. L. Gerald, W. Bornmann, J. F. Bromberg, *Breast Cancer Res.* **2007**, *9*, R32.
- [3] J. Abdulghani, L. Gu, A. Dagvadorj, J. Lutz, B. Leiby, G. Bonuccelli, M. P. Lisanti, T. Zellweger, K. Alanen, T. Mirtti, T. Visakorpi, L. Bubendorf, M. T. Nevalainen, *Am. J. Pathol.* **2008**, *172*, 1717–1728.
- [4] W. M. Burke, X. Jin, H.-J. Lin, M. Huang, R. Liu, K. R. Reynolds, J. Lin, *Oncogene* **2001**, *20*, 7925–7934.
- [5] M. Carro, W. K. Lim, M. J. Alvarez, R. J. Bollo, X. Zhao, E. Y. Snyder, E. P. Sulman, S. L. Anne, F. Doetsch, H. Colman, A. Lasorella, K. Aldape, A. Califano, A. Iavarone, *Nature* **2010**, *463*, 318–325.

- [6] H. Akca, M. Tani, T. Hishida, S. Matsumoto, Yokota, *J. Lung Cancer* **2006**, *54*, 25–33.
- [7] a) G. Inghirami, R. Chiarle, W. J. Simmons, R. Piva, K. Schlessinger, D. E. Levy, *Cell Cycle* **2005**, *4*, 1131–1133; b) K. Schlessinger, D. E. Levy, *Cancer Res.* **2005**, *65*, 5282–5834.
- [8] J. Bromberg, J. E. Darnell, Jr., *Oncogene* **2000**, *19*, 2468–2473.
- [9] J. F. Bromberg, M. H. Wrzeszczynska, G. Devagan, Y. Zhao, R. G. Pestell, C. Albanese, J. E. Darnell, Jr., *Cell* **1999**, *98*, 295–303.
- [10] a) S. Fletcher, J. Turkson, P. T. Gunning, *ChemMedChem* **2008**, *3*, 1159–1168; b) S. Fletcher, J. Drewry, V. Shahani, B. D. G. Page, P. T. Gunning, *Biochem. Cell Biol.* **2009**, *87*, 825–833; c) B. D. G. Page, D. Ball, P. T. Gunning, *Expert Opin. Ther. Pat.* **2011**, *21*, 1–19; d) S. Haftchenary, M. Avadiansian, P. T. Gunning, *Anti-Cancer Drugs* **2011**, *22*, 115–127.
- [11] K. A. Z. Siddiquee, P. T. Gunning, M. Glenn, W. P. Katt, S. Zhang, C. Schroeck, S. M. Sebti, R. Jove, A. D. Hamilton, J. Turkson, *ACS Chem. Biol.* **2007**, *12*, 787–798.
- [12] a) M. Schröder, K. Kroeger, H. D. Volk, K. A. Eidne, G. Grütz, *J. Leukoc. Biol.* **2004**, *75*, 792–797; b) P. B. Sehgal, *Semin. Cell Dev. Biol.* **2008**, *19*, 329–340.
- [13] V. Paillard, A. Kaptein, M. Saunders, *J. Biol. Chem.* **1996**, *271*, 5961–5964.
- [14] T. Faruqi, D. Gomez, X. Bustelo, D. Bar-Sagi, N. Reich, *Proc. Natl. Acad. Sci. USA* **2001**, *98*, 9014–9019.
- [15] a) J. Turkson, D. Ryan, J. S. Kim, Y. Zhang, Z. Chen, E. Haura, A. Laudano, S. M. Sebti, A. D. Hamilton, R. Jove, *J. Biol. Chem.* **2001**, *276*, 45443–45455; b) Z. Ren, L. A. Cabell, T. S. Schaefer, J. S. McMurray, *Bioorg. Med. Chem. Lett.* **2003**, *13*, 633–636.
- [16] a) J. Turkson, J. S. Kim, S. Zhang, J. Yaun, M. Haung, Glenn, M. P. E. Haura, S. M. Sebti, J. Turkson, A. D. Hamilton, *Mol. Cancer Ther.* **2004**, *3*, 261–269; b) P. K. Mandal, P. A. Heard, Z. Ren, X. Chen, J. S. McMurray, *Bioorg. Med. Chem. Lett.* **2007**, *17*, 654–656; c) J. Chen, L. Bai, D. Bernard, Z. Nikolovska-Coleska, C. Gomez, J. Zhang, H. Yi, S. Wang, *ACS Med. Chem. Lett.* **2010**, *1*, 85–89; d) P. T. Gunning, W. P. Katt, M. P. Glenn, K. A. Z. Siddiquee, J. S. Kim, R. Jove, S. M. Sebti, J. Turkson, A. D. Hamilton, *Bioorg. Med. Chem. Lett.* **2007**, *17*, 1875–1878; e) D. R. Coleman IV, K. Kaluarachchi, Z. Ren, X. Chen, J. S. McMurray, *Int. J. Pept. Res. Ther.* **2008**, *14*, 1–9; f) J. Dourlat, B. Valentin, W.-C. Liu, C. Garbay, *Bioorg. Med. Chem. Lett.* **2007**, *17*, 3943–3946; g) J. Chen, Z. Nikolovska-Coleska, C.-Y. Yang, C. Gomez, W. Gao, K. Krajewski, S. Jiang, P. Roller, S. Wang, *Bioorg. Med. Chem. Lett.* **2007**, *17*, 3939–3942; h) V. M. Shahani, P. Yue, S. Fletcher, S. Sharmeen, M. A. Sukhai, D. P. Luu, X. Zhang, H. Sun, W. Zhao, A. D. Schimmer, J. Turkson, P. T. Gunning, *Bioorg. Med. Chem.* **2011**, *19*, 1823–1838.
- [17] a) J. Schust, B. Sperl, A. Hollis, T. U. Mayer, T. Berg, *Chem. Biol.* **2006**, *13*, 1235–1242; b) L. Lin, B. Hutzen, P.-K. Li, S. Ball, M. Zuo, S. DeAngelis, E. Foust, M. Sobo, L. Friedman, D. Bhasin, L. Cen, C. Li, J. Lin, *Neoplasia* **2010**, *12*, 39–50; c) H. Song, R. Wang, S. Wang, J. Lin, *Proc. Natl. Acad. Sci. USA* **2005**, *102*, 4700–4705; d) P. T. Gunning, M. Glenn, K. A. Z. Siddiquee, W. P. Katt, E. Masson, S. M. Sebti, J. Turkson, A. D. Hamilton, *ChemBioChem* **2008**, *9*, 2800–2803; e) K. A. Z. Siddiquee, P. T. Gunning, M. Glenn, W. P. Glenn, S. M. Sebti, R. Jove, A. D. Hamilton, J. Turkson, *ACS Chem. Biol.* **2007**, *12*, 787–796; f) K. Siddiquee, S. Zhang, W. C. Guida, M. A. Blaskovich, B. Greedy, H. R. Lawrence, M. L. R. Yip, R. Jove, M. M. Laughlin, N. J. Lawrence, S. M. Sebti, J. Turkson, *Proc. Natl. Acad. Sci. USA* **2007**, *104*, 7391–7396; g) S. Fletcher, J. Singh, X. Zhang, P. Yue, Page, B. D. G., S. Sharmeen, V. M. Shahani, W. Zhao, A. D. Schimmer, J. Turkson, P. T. Gunning, *ChemBioChem* **2009**, *10*, 1959–1964; h) V. M. Shahani, P. Yue, S. Haftchenary, W. Zhao, J. Lukkarila, X. Zhang, D. Ball, C. Nona, P. T. Gunning, J. Turkson, *ACS Med. Chem. Lett.* **2011**, *2*, 79–81.
- [18] a) J. Turkson, S. Zhang, J. Palmer, H. Kay, J. Stanko, L. B. Mora, S. Sebti, H. Yu, R. Jove, *Mol. Cancer Ther.* **2004**, *3*, 1533–1542; b) J. Turkson, S. Zhang, L. B. Mora, S. Sebti, R. Jove, *J. Biol. Chem.* **2005**, *280*, 32979–32988.
- [19] G. Jones, P. Willett, R. C. Glen, A. C. Leach, R. Taylor, *J. Mol. Biol.* **1997**, *267*, 727–748.
- [20] S. Zhang, Z. Y. Zhang, *Drug Discovery Today* **2007**, *12*, 373–381.
- [21] T. Maegawa, Y. Fujita, A. Sakurai, A. Akashi, M. Sato, K. Oono, H. Sajiki, *Chem. Pharm. Bull.* **2007**, *55*, 837–839.
- [22] P. N. Pandey, M. L. Purkayastha, *Synthesis* **1982**, 876–878.
- [23] S. Fletcher, P. T. Gunning, *Tetrahedron Lett.* **2008**, *49*, 4817–4819.
- [24] C. Valerio, F. Moulines, J. Ruiz, J.-C. Blais, D. Astruc, *J. Org. Chem.* **2000**, *65*, 1996–2002.
- [25] J. Schust, T. Berg, *Anal. Biochem.* **2004**, *330*, 114–118.
- [26] P. Wu, M. Brasseur, U. Schindler, *Anal. Biochem.* **1997**, *249*, 29–36.
- [27] W. Zhao, S. Jaganathan, J. Turkson, *J. Biol. Chem.* **2010**, *285*, 35855–35865.
- [28] F. Alimirah, J. Chen, Z. Basrawala, H. Xin, D. Choubey, *FEBS Lett.* **2006**, *580*, 2294–2300.
- [29] C. Wang, J. E. Curtis, M. D. Minden, E. A. McCulloch, *Leukemia* **1989**, *3*, 264–269.
- [30] D. A. N. Carlesso, Frank, J. D. Griffin, *J. Exp. Med.* **1996**, *183*, 811–820.

Received: April 16, 2011

Published online on May 25, 2011